Metallic Implants in MRI – Hazards and Imaging Artifacts

Metallische Implantate im MRT – Gefahren und Bildartefakte

Authors

Eva Peschke[1], Patricia Ulloa[2], Olav Jansen[2], Jan-Bernd Hoevener[1]

Affiliations

1 Department for Radiology and Neuroradiology, Molecular Imaging North Competence Center (MOIN CC), Section Biomedical Imaging, University Hospital Schleswig-Holstein – Campus Kiel, Kiel University, Germany

2 Department of Radiology and Neuroradiology, University Hospital Schleswig-Holstein – Campus Kiel, Germany

Correspondence

Eva Peschke
Radiology and Neuroradiology, University Hospital Schleswig-Holstein Campus Kiel Biomedical Imaging Section,
Am Botanischen Garten 14, 24118 Kiel, Germany
Tel.: +49/4 31/8 80 58 39
eva.peschke@rad.uni-kiel.de

Jan-Bernd Hövener
Radiology and Neuroradiology, University Hospital Schleswig-Holstein Campus Kiel Biomedical Imaging Section,
Am Botanischen Garten 14, 24118 Kiel, Germany
Tel.: +49/4 31/8 80 58 39
Jan.Hoevener@rad.uni-kiel.de

ZUSAMMENFASSUNG

Hintergrund Die Magnetresonanztomografie (MRT) ist eine Untersuchungsmethode für die nichtinvasive Bildgebung der Weichteile ohne die Verwendung von ionisierender Strahlung. Metallische Implantate können jedoch ein Risiko für den Patienten darstellen und führen häufig zu Bildgebungsartefakten. Aufgrund der steigenden Anzahl von Implantaten ist die Reduzierung dieser Artefakte zu einem wichtigen Ziel geworden. In dieser Übersichtsarbeit beschreiben wir die mit Implantaten und MRT verbundenen Risiken und liefern den Hintergrund, wie metallinduzierte Artefakte entstehen. Wir erläutern die gängigen Methoden zur Artefaktreduktion aus der Literatur und fassen diese zusammen.

Methoden Für diese Übersichtsarbeit wurde eine PubMed-Literatursuche mit den Stichworten „MRI metal artefact reduction", „metallic implants" und „MRI artefacts/artifacts" durchgeführt.

Ergebnisse und Schlussfolgerung Die MRT-Verträglichkeit von Implantaten muss individuell bewertet werden. Zur Reduzierung von Artefakten wurden 2 generelle Ansätze gefunden: a) Parameteroptimierung in Standardsequenzen (Echozeit, Schichtdicke, Bandbreite) und b) spezialisierte Sequenzen wie VAT, OMAR, WARP, SEMAC und MAVRIC. Diese Methoden reduzierten Artefakte und verbesserten die Bildqualität, wenn auch auf Kosten einer (manchmal deutlich) verlängerten Scanzeit. Neue Entwicklungen in der beschleunigten Bildgebung werden die Scanzeit dieser Methoden wahrscheinlich deutlich verkürzen, sodass ein routinemäßiger Einsatz möglich werden könnte.

Kernaussagen:

- Metallische Implantate können ein Risiko für Patienten darstellen und verursachen oft Artefakte.
- Bildartefakte können durch Parameteroptimierung und spezielle Sequenzen reduziert werden.
- Metallartefakte werden durch kürzere TE, kleinere Voxelgröße, größere Bildmatrix und größere Bandbreite reduziert.
- SPI, STIR, VAT, SEMAC, MAVRIC und MAVRIC-SL sind spezialisierte MRT-Sequenzen, die Artefakte weiter reduzieren können.

ABSTRACT

Background Magnetic resonance imaging (MRI) is an examination method for noninvasive soft tissue imaging without the use of ionizing radiation. Metallic implants, however, may pose a risk for the patient and often result in imaging artifacts. Due to the increasing number of implants, reducing these artifacts has become an important goal. In this review, we describe the risks associated with implants and provide the background on how metal-induced artifacts are formed. We review the literature on methods on how to reduce artifacts and summarize our findings.

Method The literature was searched using PubMed and the keywords "MRI metal artifact reduction", "metallic implants" and "MRI artefacts/artifacts".

Results and Conclusion The MRI compatibility of implants has to be evaluated individually. To reduce artifacts, two general approaches were found: a) parameter optimization in standard sequences (echo time, slice thickness, bandwidth) and b) specialized sequences, such as VAT, OMAR, WARP, SEMAC and MAVRIC. These methods reduced artifacts and improved image quality, albeit at the cost of a (sometimes significantly) prolonged scan time. New developments in accelerated imaging will likely shorten the scan time of these methods significantly, such that routine use may become feasible.

Key Points:

- Metallic implants may pose a risk for patients and often cause artifacts.
- Imaging artifacts can be reduced by parameter optimization or special sequences.
- Metal artifacts are reduced with a lower TE, smaller voxel size, larger matrix, and higher bandwidth.
- SPI, STIR, VAT, SEMAC, MAVRIC, and MAVRIC-SL are specialized MR sequences that can reduce artifacts further.

The recent decades have seen a dramatic development in medical technologies. Both diagnostic and treatment options have multiplied and become more accessible. Magnetic resonance imaging (MRI), for instance, has become the gold standard for noninvasive tomographic soft tissue imaging, e. g. for treatment monitoring [1].

MRI features excellent soft tissue contrast and unparalleled rich contrasts, while at the same time requiring no ionizing radiation. MRI is generally widely applicable and there are only a few contraindications, e. g., claustrophobia and some implants.

The latter point is of particular interest because more and more medical implants are being used as treatment options [2]. Examples include active devices such as pacemakers and insulin pumps, or passive ones like metallic screws, nails, stents, and joint replacements.

MRI and implants, however, are not always compatible. They may pose a threat to the patient and affect image quality. These artifacts may cause visual distortions in the MR image, signal voids, or signal pile-ups [3], thereby greatly affecting the diagnostic quality of the image. To address this issue, various approaches have been developed.

This review discusses the hazards and artifacts of implants and current approaches to reduce the latter. The goal is to provide the reader with an understanding of the topic that is sufficient for using and optimizing sequences for imaging implants.

Hazards

In general, MRI examinations are considered relatively safe for the patient and less harmful than, for example, X-rays. Hazards of routine MRI include heating, the attraction of loose ferromagnetic objects, peripheral nerve stimulation, and claustrophobia [4]. Special care has to be taken with respect to implants. Decisions as to whether or not a patient with an implant can undergo MRI have to be made on an individual basis. There are three classifications for implants with respect to MRI: MRI-safe, MRI-unsafe and MRI-conditional [5]. The information is usually provided in the implant user instructions (according to the international electro-technical commission IEC 60 601–2-33 2010) or third-party services [6, 7].

MR-safe implants are not considered to pose a significant risk for patients undergoing MRI. Implants are categorized as MR-unsafe mostly because of the use of ferromagnetic materials. Patients with MR-unsafe implants cannot undergo MRI. MRI-conditional implants can be scanned under certain conditions (see instructions for use [8]). Still, specific handling is required, e. g. limits of the magnetic or radiofrequency field or a certain specific absorption rate must not be exceeded [5].

Hazards of implants with respect to MRI include malfunction (e. g., pacemakers) or harm by displacement, heating, or induced voltages. These effects are caused by the strong, static magnetic field $B_0 \approx 1\,T$, weaker but rapidly changing magnetic fields (gradients) $B_G \approx 10^{-3}\,T$ at a frequency in the kHz range, and radiofrequency (RF) fields $B_1 \approx 10^{-6}\,T$ with a frequency in the 10–200 MHz range. In the following, we briefly describe the hazards caused by the different fields with a focus on implants.

Static magnetic field

Most modern MRI systems feature a magnetic field B_0 of 1.5 or 3 T. As per convention, we assume the main component of the static magnetic field to be in the z-direction along the bore (Equation 1).

$$\mathbf{B}_0 = [0, 0, B_z] \tag{1}$$

The static magnetic field can attract loose ferromagnetic objects. Therefore, care has to be taken that no ferromagnetic material is brought near the MRI. In the past, fatal accidents have occurred when large metallic objects were attracted by the magnetic field and hit patients [4, 9]. This includes items of daily use in the hospital such as oxygen cylinders (▶ **Fig. 1**), patient beds, scissors, and cleaning utensils. Accidents have also been caused on rare occasions, e. g., by respiratory equipment of firefighters.

In general, materials are divided into three different classes depending on the magnetic susceptibility (χ): diamagnetic (χ < 0), paramagnetic (χ > 0) and ferromagnetic (χ >> 1) materials. The magnetic susceptibility is a property that indicates how strongly a material will be magnetized by an external magnetic field [10].

► **Fig. 1** Photograph of an oxygen bottle in a 3 T whole-body MRI unit. A non-MR-safe oxygen bottle was carried into the MRI room and attracted by the strong magnetic field causing it to be catapulted into the MRI unit.

► **Abb. 1** Foto einer Sauerstoffflasche in einem 3T-Ganzkörper-MRT. Eine nicht MR-sichere Sauerstoffflasche wurde in den MRT-Raum getragen und durch das starke Magnetfeld so angezogen, dass sie in die MRT-Röhre katapultiert wurde.

Implants containing ferromagnetic material will exert a force, leading to displacement of the implant and thus malfunctioning or tissue injury.

Gradient fields

When exposed to changing magnetic fields, a voltage is induced into a conductor. This voltage results in a current if the resistance is finite. For MRI, changing magnetic fluxes occur while approaching B_0 (the magnet) and by rapidly switching, spatially varying magnetic field B_G ("gradients"). Gradients are applied in each Cartesian direction (Equation 2):

$$\mathbf{B}_G = [B_{GX}, B_{GY}, B_{GZ}] \tag{2}$$

While entering the bore is relatively harmless, vertigo has been reported, especially at ultra-high fields of 7 T [11]. Gradients may induce electrical stimulation of nerves [12] or even heating of tissue [13].

In most cases, the unintentional nerve excitation is an uncomfortable but transient sensation for the patient (e. g., twitching or tingling). However, external devices, such as electrodes, may heat up significantly and cause fourth-degree burns [14]. To avoid burns, skin-skin contact (e. g., touching hands, thighs) or skin-metal contact has to be prevented [4]. For active implants, induced voltages could result in damaged circuits or malfunction like unwanted impulses (e. g., pacemaker) [15]. To account for the effects of switching gradients, some MR-conditional implants are specified to a maximal allowed slew rate. The slew rate of a gradient is a measure for how fast a gradient is turned on (in units of Tesla per meter per second (T/m/s)). It is calculated by the ratio of the maximum value of the gradient and the time necessary to reach this gradient amplitude.

RF pulses

Radiofrequency (RF) pulses applied by every MRI are partially absorbed by the tissue and converted to heat. The rate, how much energy is absorbed, is given by the specific absorption rate (SAR) in units of W/kg and depends on the patient's size and body weight. To avoid heating, the allowed SAR must not be exceeded.

Conductive materials, like some implants, may reflect and absorb the RF pulses and thus increase heating [16]. Each implant is approved for a given magnetic field strength and SAR, e. g. 1.5 T and SAR < 2.0 W/kg for cardiovascular devices [17] or 1.5 T and SAR < 0.1 W/kg for deep brain stimulations [16]. However, it was realized that SAR is not the optimum measure to access implant safety. Instead, the root mean of the B_1 field (B_1+rms in units of mT) was suggested. B_1+rms does not depend on the patient and is used for accessing implant safety today [18, 19].

Imaging artifacts

Often, implants contain magnetic materials that distort the static magnetic field and shield RF pulses. This distortion is caused by the magnetic susceptibility (χ) that is much different compared to the surrounding tissue (see the previous section). This distortion results in an altered resonance frequency of the spins in the affected volume. These frequency changes may have several effects: a) the spins are not excited and/or detected, b) a fast $T2^*$ decay and c) errors in the spatial localization. To understand these effects, we need to consider the physical background of an MRI sequence.

Magnetization and resonance frequency

The nuclei (protons) of hydrogen atoms like in water (H_2O) possess a nuclear spin, which gives rise to a magnetic moment. The spin is a quantum mechanical property, which we do not need to consider in much detail for the purposes of this paper. It is essential to consider, however, that the spins have two stationary states in a magnetic field, parallel ("up") or antiparallel ("down"). One milligram of water, 1 mm³, contains approx. 10^{20} hydrogen atoms and thus spins and their magnetic moments.

However, most of these spins are MR-invisible and do not contribute to the MRI signal because they are almost equally in the up and down state and effectively cancel each other out (Boltzmann distribution of the Zeemann states). Only a small fraction of all spins, called polarization P, contributes to the magnetization and thus signal (Equation 3). The approximation only holds for room temperature

$$P = \frac{N\uparrow - N\downarrow}{N\uparrow + N\downarrow} = \tanh\left(\frac{\hbar\gamma B_0}{2kT}\right) \approx \frac{\hbar\gamma B_0}{2kT} \tag{3}$$

At room temperature, P and thus the magnitude of **M** increase approx. linearly with the strength of an outer magnetic field B_0. This is the reason why ever stronger magnets are being built.

Still, the polarization is very small – no more than about three parts per million (ppm) effectively contribute the signal at 1 T (or ≈ 10 ppm at 3 T). Thus, 99.999 percent of all spins are invisible at current magnetic fields. This implies that 100 000-fold en-

hancements are possible by increasing polarization – a fact that hyperpolarization techniques exploit [20]. Still, the small fraction of spins contributing to the signal is sufficient for MRI as we know it today.

Leaving the microscopic scale, let's consider that the spins, e.g., of 1 mm³ water, form a macroscopic magnetization vector $\mathbf{M} = [M_x \ M_y \ M_z]$. Some aspects of this macroscopic magnetization may be compared to the needle of a hiking compass. One gram of water has a nuclear magnetization of 3.1 A/m in a magnetic field of 1 T. With $\mathbf{B}_0 = [0, 0, B_z]$, the magnetization becomes $\mathbf{M} = [0, 0, M_z]$.

When an oscillating magnetic field $\mathbf{B}_1$ is applied at the right frequency ω_L and perpendicular to $\mathbf{B}_0$, magnetization $\mathbf{M}$ can be excited or flipped by an arbitrary degree α. The energy difference between the up- and downstate is dependent on the Larmor frequency ω_L:

$$\omega_L = \gamma B_0 \tag{4}$$

$$\alpha = \gamma B_1 t_{RF} \tag{5}$$

Where γ is the magnetogyric ratio, a constant of nature proportional to the magnetic moment of the element under consideration ($\gamma(^1H) = 42$ MHz/T 2π), and t_{RF} is the duration of the RF pulse. Note: ω_L is directly proportional to B_0.

It is important to note that the excitation pulse has a finite bandwidth bw_p – that is a frequency range, where the excitation pulse affects the magnetization. A higher bandwidth corresponds to a larger frequency range and therefore excites spins across a broader range of Larmor frequencies. The bandwidth depends on the duration and shape of the pulse.

After the excitation pulse, the magnetization vectors $\mathbf{M}$ precess about the z-axis. Any component of the magnetization vector in the xy-plane, $[M_x \ M_y]$, induces an alternating magnetic flux and thus a current in a nearby conductor (e.g., a coil): this is the MR signal.

Similar to the excitation, the detection process has a bandwidth bw_d, too, which depends on the rate of the discrete sampling of the continuous MR signal

$$bw_d = \frac{1}{t_d} \tag{6}$$

where t_d is the dwell time and depicts the interval between two digitized samples. Shorter sampling intervals result in a higher bandwidth but reduce the signal-to-noise ratio (SNR) because less time was used to collect the signal. Different vendors indicate the bandwidth differently, either the total bandwidth in Hz or the bandwidth divided by the number of steps for the frequency encoding in bandwidth in Hz/Px.

After the excitation, the longitudinal or z-component of the magnetization M_z returns to its equilibrium value, M_0, while M_{xy} decays to zero. Both effects can be described with exponential functions with the constant T1 for longitudinal and T2, T2* and T2$_i$ for transverse relaxation (Equation 7). Once M_{xy} is zero, no MR signal is recorded (while M_z may not yet be recovered). There are two fundamental effects contributing to the transverse relaxation: the effect of static B_0 inhomogeneities, described by an exponential decay with T2$_i$, and other components, described by

T2. While the T2 decay is irreversible, loss by T2$_i$ decay can be recovered by refocusing the magnetization in spin echoes.

Spin echoes are formed by flipping the transverse magnetization around x or y. This way, the effect of the inhomogeneities is reversed.

$$\frac{1}{T2^*} = \frac{1}{T2_i} = \frac{1}{T2} \tag{7}$$

For spatial encoding, i.e., imaging, additional magnetic fields, $\mathbf{B}_G$, are applied whose strengths vary with the position in space:

$$\mathbf{B}_G = [G_x x, \ G_y y, \ G_z z] \tag{8}$$

G_x, G_y and G_z are the strength of the gradient fields in T/m and x, y and z are the spatial positions in m.

$\mathbf{B}_G$ is applied at different points in time: during the pulse ("slice selection"), between excitation and detection ("phase encoding"), or during readout ("readout encoding").

It is essential to realize that the magnetic field's linear variation (induced by $\mathbf{B}_G$) causes a spatial dependency of the Larmor frequency. As a result, the Larmor frequency becomes a function of the position, and this relation of spatial location and resonance frequency allows the reconstruction of images. Using this effect for imaging was awarded the Nobel Prize in 2003.

It should be noted that when we talk about the strength of an MRI device, we refer to the magnetic flux density, $\mathbf{B}$, in T and not to the magnetic field strength, $\mathbf{H}$, in A/m. The permeability, a proportionality factor, connects B and H.

Impact of implants

As mentioned above, implants are either paramagnetic, diamagnetic, or ferromagnetic, a classification depending on their magnetic susceptibility χ. Like implant materials, each tissue in the body also has a different magnetic susceptibility (▶ **Table 1**).

Material brought into a magnetic field may enhance, weaken, or not affect the magnetic field locally (▶ **Fig. 2**).

Diamagnetic material, such as biological tissue and calcium, will weaken the magnetic field, while paramagnetic and ferromagnetic material, like gadolinium and iron, will enhance the magnetic field locally. The susceptibilities of different tissues are similar enough to have little impact on conventional MRI, although specialized sequences generate contrast based on different susceptibilities (susceptibility-weighted imaging, SWI) [21]. Problems occur in the presence of metal implants or at the interface between air and tissue (e.g., nasal cavities, intestines).

For implants, due to the different magnetic susceptibility compared to surrounding tissue, the magnetic field is distorted, causing changes in the Larmor frequency of nearby spins. This may have one or all of the following effects:
1. Insufficient excitation because ω_L is not within bw_p
2. Low signal detection because ω_L is outside of bw_d
3. Low signal detection because the transverse magnetization decays very fast (large T2', dephasing)
4. Misregistration of spins because ω_L is different than expected (▶ **Fig. 3**).
5. Failure of frequency selective pulses.
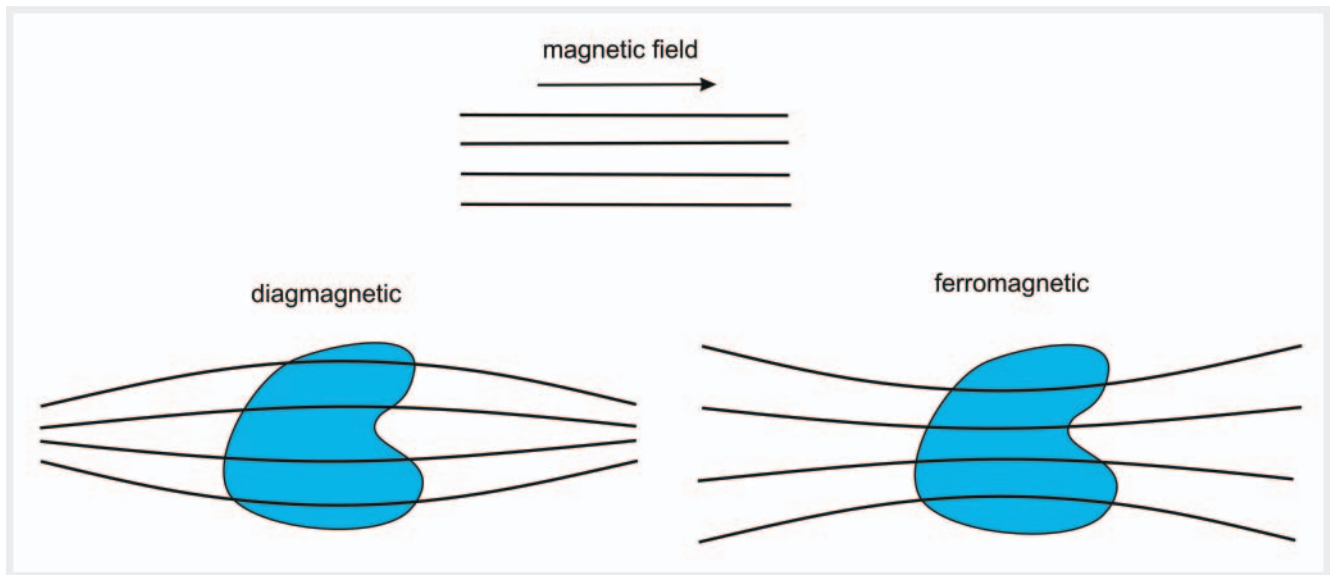
▶ **Fig. 2** Schematic of the influence of diamagnetic or paramagnetic/ferromagnetic material on the magnetic field. Diamagnetic materials weaken the magnetic field, while paramagnetic and ferromagnetic materials enhance the magnetic field.

▶ **Abb. 2** Schematische Darstellung des Einflusses von diamagnetischem oder paramagnetischem/ferromagnetischem Material auf das Magnetfeld. Diamagnetische Materialien schwächen das Magnetfeld, während paramagnetische und ferromagnetische Materialien das Magnetfeld verstärken.

▶ **Table 1** Typical magnetic susceptibilities (χ) for different materials and the corresponding magnetic properties.

▶ **Tab. 1** Typische magnetische Suszeptibilitäten (χ) für verschiedene Materialien und die entsprechenden magnetischen Eigenschaften.

material	magnetic susceptibility (χ)	magnetic property
silver	-20×10^{-6}	diamagnetic
water, soft tissue	-9.05×10^{-6}	diamagnetic
bone	-8.86×10^{-6}	diamagnetic
magnesium	11.7×10^{-6}	paramagnetic
titanium	182×10^{-6}	paramagnetic
air	0.36×10^{-6}	paramagnetic
iron	$\sim 10^{5}$	ferromagnetic
magnetic stainless steel	$\sim 10^{3}$	ferromagnetic

All of this will lead to signal loss or signal pile-up and cause spatial distortions in the measured slice.

In addition to image distortion, failure of spectral fat suppression often occurs in tissue near metal implants for the same reason (distortions of the magnetic field and thus Larmor frequencies). Spectral fat suppression methods use the fact that the Larmor frequencies (chemical shift) of water and fat are different by approximately 3.5 ppm (e. g., 220 Hz for 1.5 T). A narrow (low bw_p) pulse is applied at the frequency of fat to saturate its magnetization to suppress the fat signal. In the proximity of metal im-

plants, the field and thus frequencies are distorted (e. g., by 30–80 Hz). As a result, fat is not excited by the narrow saturation pulses. Similar effects occur in other techniques, such as Dixon-type fat water imaging [22] (▶ **Fig. 4**).

Reduction of imaging artifacts

Several approaches were suggested to reduce implant-related artifacts. To some extent, standard sequences can be used with some parameter optimization. Additionally, special MRI sequences were developed for artifact reduction. In general, artifacts are dependent on the field strength of the MRI device, the used sequence, the chosen parameters, and the properties of the implant itself, such as orientation and type of material.

General considerations

Lower magnetic field strengths exhibit less metal-induced artifacts than higher field strengths. The field homogeneity (also without an implant) is higher in lower magnetic fields. Thus, lower field strengths were recommended for imaging implants [23–34].

As expected, the material's susceptibility was found to affect the artifacts: larger susceptibility differences caused larger distortions.

The orientation of the implant with respect to B_0 may play a role, too [35]. It appears beneficial to position the long implant axis parallel to B_0, although it must not act as an antenna as heating may occur.

The phase encoding direction is less affected by metal artifacts. Thus, it may be advantageous to switch the phase and frequency encoding direction to improve the visibility of the nearby tissue. If phase oversampling is needed to avoid a folding artifact, the measurement time increases [22, 25].
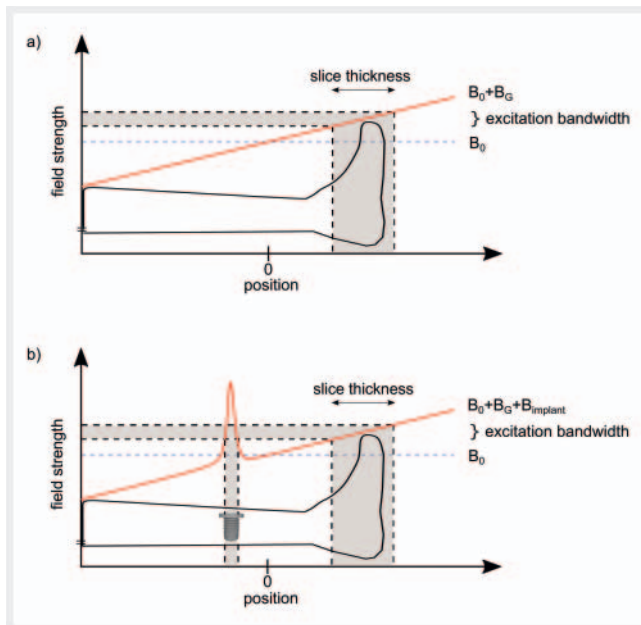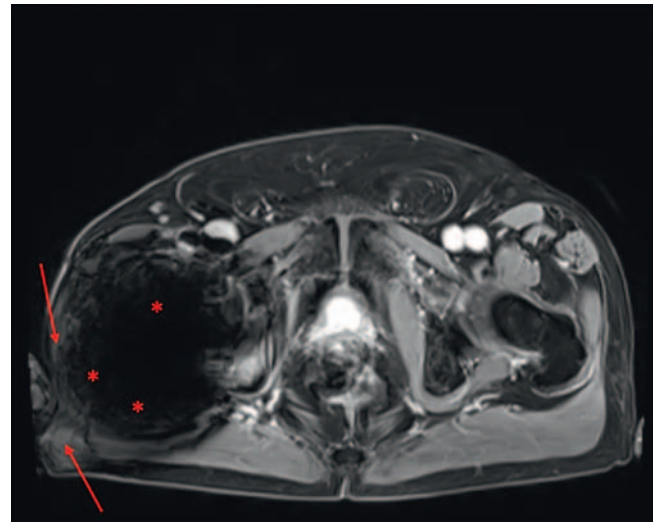
▶ **Fig. 3** Schematic view of signal pile-up induced by implants: The superposition of B_0 (dashed line) and B_G cause the field strength to vary linearly with the position (red line, top). When a pulse is applied, all spins within the excitation bandwidth of the pulse ($f_p \pm bw_p/2$) are excited. As a result, only spins within a slice are excited (shaded areas). If the field is distorted, e. g., by an implant (red line, bottom), the variation of the field strength is not linear due to Bimplant. Therefore, other spins outside that slice may contribute to the signal, too, causing so-called pile-up artifacts.

▶ **Abb. 3** Schematische Darstellung der durch Implantate induzierten Signalanhäufung: Die Überlagerung von B_0 (gestrichelte Linie) und B_G bewirkt, dass die Feldstärke linear mit der Position variiert (rote Linie, oben). Wird ein Puls angelegt, werden alle Spins innerhalb der Anregungsbandbreite des Pulses ($f_p \pm bw_p/2$) angeregt. Dadurch werden nur Spins innerhalb einer Schicht angeregt (schattierte Bereiche). Wird das Feld z. B. durch ein Implantat verzerrt (rote Linie, unten), ist die Variation der Feldstärke aufgrund des Implantats nicht linear. Daher können auch andere Spins außerhalb dieser Schicht zum Signal beitragen, was zu sogenannten Pile-up-Artefakten führt.

▶ **Fig. 4** Reconstruction of a fat-suppressed, abdominal T1-weighted 3D gradient echo Dixon MRI of a patient with an artificial hip joint (left). The implant caused signal loss (*) as well as failure of fat-water separation (arrows). No such artifacts are apparent on the other side.

▶ **Abb. 4** Rekonstruktion eines fettunterdrückten, abdominalen, T1-gewichteten 3D-Gradientenecho-Dixon-MRTs eines Patienten mit einem künstlichen Hüftgelenk (links). Das Implantat verursacht einen Signalverlust (*) sowie ein Versagen der Fett-Wasser-Trennung (Pfeile). Auf der anderen Seite sind keine derartigen Artefakte zu erkennen.
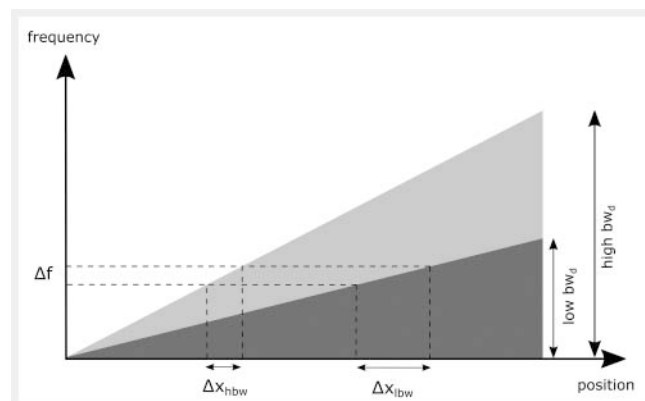
▶ **Fig. 5** Schematic of different receiver bandwidths (bw_d) on spatial distortions (Δx). In the case of a frequency offset due to field inhomogeneities, a higher receiver bandwidth results in smaller spatial distortion than lower receiver bandwidths.

▶ **Abb. 5** Schematische Darstellung unterschiedlicher Empfangsbandbreiten (bw_d) auf die räumliche Verzerrung (Δx). Bei einem Frequenzunterschied aufgrund von Feldinhomogenitäten führen höhere Empfängerbandbreiten zu geringeren räumlichen Verzerrungen im Vergleich zu niedrigeren Empfängerbandbreiten.

Some sequence types are more robust with respect to distortions than others. Generally, spin echo (SE) sequences are benign because the echo can be acquired fully, even if T2* is short (compared to gradient echo sequences, where the signal may decay with T2* during spatial encoding before the acquisition is started). As a result, some of the inhomogeneities can be refocused with spin echo sequences. Although spin-echo-based sequences have benefits, some sequences like phase contrast imaging or fast imaging methods often use gradient echoes. Here, it is advantageous to reduce the time between excitation and image acquisition, TE [28, 29, 32, 36, 37]. In the extreme, ultra-short or zero-TE sequences can reduce artifacts and even image hard tissues [38, 39].

In the presence of field inhomogeneities, the spins precess with a frequency offset of Δf compared to the non-distorted case. The spatial distortion depends on the frequency offset and the slice thickness and negatively on the excitation bandwidth (bw_p) [22]. Besides this, the spatial distortion also depends on the receiver bandwidth (bw_d). A higher receiver bandwidth reduces the spatial distortion (▶ Fig. 5) as well as an increasing slice selection gradient, which results in a decreased slice thickness. Additionally, increasing the matrix size or reducing the voxel size is helpful for reducing metal artifacts. However, a drawback of those reduction tech-
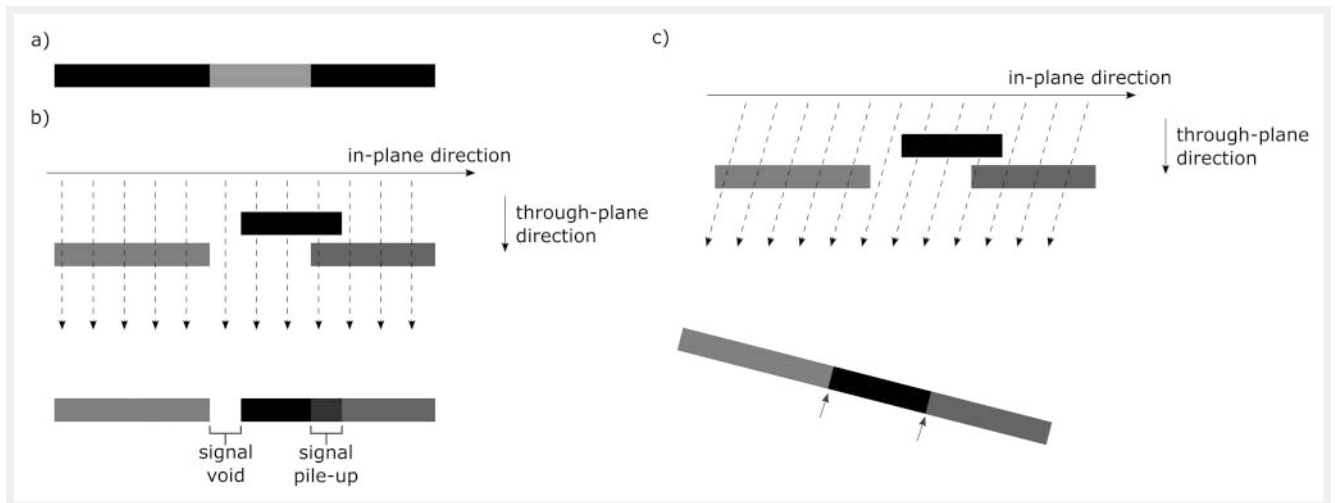
▶ **Fig. 6** Schematic of the principle of view-angle tilting (VAT). **a** non-distorted field, **b** distorted field without correction, and **c** distorted field with VAT. The distortion in **b** results in a signal void and signal pile-up in the measured slice due to the inhomogeneities. The angle of the readout direction **c** reduces the distortion but results in blurring edges (blue arrows).

▶ **Abb. 6** Schematische Darstellung des Prinzips des view-angle tilting (VAT). **a** keine Feldverzerrung, **b** Feldverzerrung ohne Korrektur und **c** Feldverzerrung mit VAT. Aufgrund der Inhomogenitäten führt die Verzerrung in **b** zu einer Signalauslöschung und Signalanhäufung in der gemessenen Schicht. Der Winkel der Ausleserichtung **c** reduziert die Verzerrung, führt aber zu unscharfen Kanten (blaue Pfeile).

niques is an increased scan time and reduced signal-to-noise ratio (SNR) [24, 25, 34, 36, 37, 40, 41]. A higher slice selection gradient ensures that each slice is encoded with a higher frequency range. As a result, spins with higher or lower Larmor frequencies (e. g., caused by field inhomogeneities) are still excited in the correct slice and contribute to the signal. This especially reduces signal loss. Again, higher bandwidth reduces SNR [23–25, 32, 36, 40–44]. For fat suppression near metal implants, spectral fat suppression sequences should be avoided. Instead, T1-based suppression techniques, such as short tau inversion recovery (STIR), are more robust. STIR exploits the fact that the T1-relaxation time of fat is shorter than that of tissue and can be nulled with an inversion pulse. STIR is beneficial compared to the spectral fat suppression near implants but results in a lower SNR. Additionally, a second RF pulse is necessary, which increases the specific SAR.

Special sequences with high robustness against spatial distortions

One problem regarding imaging near metal implants is the failure of slice selection and readout encoding. For the acquisition of an MR image without slice selection and readout encoding, single point imaging (SPI) can be used. In SPI sequences, only phase encoding is applied, and only one point in k-space is acquired for each excitation. This method makes it possible to minimize the time between excitation and acquisition but leads to very long scan times of 40 minutes or longer which are rarely practical for in vivo use [45].

To reduce in-plane distortions, view-angle tilting (VAT) was suggested in conjunction with spin echo sequences. VAT exploits the fact that the distortion is dependent on the gradient strength of the slice selection gradient. To compensate the off-resonance effects of the slice selection gradient, an additional gradient is used during the readout, equivalent to the one used for slice selection.

The additional gradient results in a tilting of the readout direction (▶ Fig. 6). The readout direction's tilt reduces the in-plane artifacts, but with a drawback of blurred edges [40, 42, 46, 47].

A specific optimization of parameters (high bandwidth, thin slices) was initially introduced by Olsen et al. as a metal artifact reduction sequence (MARS) [48]. More recently, modified spin echo sequences were combined with a view-angle tilting technique [49].

VAT is only able to reduce in-plane distortion. Slice Encoding for Metal Artifact Correction (SEMAC) was suggested to reduce through-plane distortions, which can be applied additionally to VAT. SEMAC is based on a conventional 2 D spin-echo sequence. It utilizes an additional phase-encoding step in the slice-selection direction, which reduces slice distortions. Knowledge of slice distortion can be used in the postprocessing step, where each slice is coded and reconstructed individually. The number of slice encoding steps is dependent on the extent of the geometric distortion. Like the other methods mentioned, this sequence's drawback is the increased scan time of around 10 minutes [37, 43, 50]. By optimizing for the particular implant, the scan time can be reduced to around 5 minutes [51].

Another sequence suggested for reducing through-plane distortions was Multi-Acquisition Variable Resonance Image Combination (MAVRIC), based on a 3D fast spin echo sequence. Here, multiple frequency-selective excitations are used instead of a single excitation pulse. All excited slabs are then analyzed in the postprocessing step to reduce artifacts. Like SEMAC, MAVRIC increases the scan time to around 20–25 min [22, 37, 52, 53].

A combination of SEMAC and MAVRIC was introduced by Koch et al. [53]. MAVRIC SL uses the selective excitation pulse like SEMAC, but the pulse profile is the same as for MAVRIC [24].

It is a common phenomenon that manufacturers give different names to relatively similar sequences. For example, optimized

spin echo sequences with VAT are called O-MAR [54] (Philips) and WARP [55] (Siemens), or O-MAR XD [56] and Advanced WARP [57] with the addition of SEMAC. Readers are advised to consult available online databases to identify the appropriate sequence for their system.

It should not go unmentioned that attempts were recently made to reduce artifacts using artificial intelligence (AI) [58, 59].

Summary

Besides the risk of injury, implants may severely influence MR image quality depending on the susceptibility of the implant. Careful selection of sequence parameters or the use of specialized solutions alleviates the issue.

If metal-induced artifacts occur, it may help to consider the following:
- Lower magnetic field strength
- Shorter TE
- Revert to spin echo sequences
- Thinner slices
- Smaller voxels
- Larger matrix size
- Higher excitation and detection bandwidth
- Switching of slice, phase, and readout direction
- Insufficient fat suppression: switch from spectral techniques to inversion techniques (e. g., STIR)

The following sequences or modules also offer some benefits:
- Single point imaging (SPI)
- UTE, ZTE
- Metal artifact reduction sequence (MARS)
- View angle tilting (VAT)
- Slice encoding for metal artifact correction (SEMAC)
- Multi-acquisition variable resonance image combination (MAVRIC)
- MAVRIC-SL

Overall, magnetic materials have always caused significant artifacts on MRI and continue doing so on modern machines. Various methods have been introduced to alleviate this issue but often come at the cost of prolonged scan times. Acceleration techniques may make these methods applicable for the clinical routine. Metal artifact reduction is an ongoing and highly relevant field of research. Undoubtedly, the future will bring more developments as more and more implants are being used, and it will become ever more important to diagnose the surrounding issue, e. g., for inflammation.

Funding

Conflict of Interest

The authors declare that they have no conflict of interest.

References

[1] Crues J, Bydder G. Frontiers in musculoskeletal imaging. Journal of Magnetic Resonance Imaging 2007; 25: 232–233. doi:10.1002/jmri.20862

[2] Kurtz S, Ong K, Lau E et al. Projections of Primary and Revision Hip and Knee Arthroplasty in the United States from 2005 to 2030. JBJS 2007; 89: 780–785. doi:10.2106/JBJS.F.00222

[3] Do T, Sutter R, Skornitzke S et al. CT and MRI Techniques for Imaging Around Orthopedic Hardware. Fortschr Röntgenstr 2018; 190: 31–41. doi:10.1055/s-0043-118127

[4] Sammet S. Magnetic resonance safety. Abdom Radiol 2016; 41: 444–451. doi:10.1007/s00261-016-0680-4

[5] Promoting Safe Use of MRI Technology | ASTM Standardization News. Im Internet (Stand: 09.07.2020): https://www.astm.org/standardization-news/?q=features/promoting-safe-use-of-mri-technology-ma12.html

[6] MRI Safety Home. Im Internet (Stand: 25.01.2021): http://mrisafety.com/

[7] Magresource. MagResource. Im Internet (Stand: 25.01.2021): https://magresource.com/

[8] Schaefers G. How to interpret and apply MR implant labeling information correctly in practice 2011; 2084 words. doi:10.1594/ECR2011/C-1886

[9] Schenck JF. Safety of Strong, Static Magnetic Fields. Journal of Magnetic Resonance Imaging 2000; 12: 2–19. doi:10.1002/1522-2586(200007)12:1<2::AID-JMRI2>3.0.CO;2-V

[10] Schenck JF. The role of magnetic susceptibility in magnetic resonance imaging: MRI magnetic compatibility of the first and second kinds. Med Phys 1996; 23: 815–850. doi:10.1118/1.597854

[11] Heilmaier C, Theysohn JM, Maderwald S et al. A large-scale study on subjective perception of discomfort during 7 and 1.5 T MRI examinations. Bioelectromagnetics 2011; 32: 610–619. doi:10.1002/bem.20680

[12] Ham CL, Engels JM, van de Wiel GT et al. Peripheral nerve stimulation during MRI: effects of high gradient amplitudes and switching rates. J Magn Reson Imaging 1997; 7: 933–937. doi:10.1002/jmri.1880070524

[13] Tokue H, Tokue A, Tsushima Y. Unexpected magnetic resonance imaging burn injuries from jogging pants. Radiol Case Rep 2019; 14: 1348–1351. doi:10.1016/j.radcr.2019.08.015

[14] Haik J, Daniel S, Tessone A et al. MRI induced fourth-degree burn in an extremity, leading to amputation. Burns 2009; 35: 294–296. doi:10.1016/j.burns.2007.11.008

[15] Mattei E, Censi F, Calcagnini G et al. Pacemaker and ICD oversensing induced by movements near the MRI scanner bore. Medical Physics 2016; 43: 6621–6631. doi:10.1118/1.4967856

[16] Erhardt JB, Fuhrer E, Gruschke OG et al. Should patients with brain implants undergo MRI? J Neural Eng 2018; 15: 041002 doi:10.1088/1741-2552/aab4e4

[17] Nordbeck P, Ertl G, Ritter O. Magnetic resonance imaging safety in pacemaker and implantable cardioverter defibrillator patients: how far have we come? Eur Heart J 2015; 36: 1505–1511. doi:10.1093/eurheartj/ehv086

[18] Baker KB, Tkach JA, Nyenhuis JA et al. Evaluation of specific absorption rate as a dosimeter of MRI-related implant heating. J Magn Reson Imaging 2004; 20: 315–320. doi:10.1002/jmri.20103

[19] Signals. Im Internet (Stand: 10.01.2021): http://www.ismrm.org/smrt/E-Signals/2016FEBRUARY/eSig_5_1_hot_2.htm

[20] Skinner JG, Menichetti L, Flori A et al. Metabolic and Molecular Imaging with Hyperpolarised Tracers. Mol Imaging Biol 2018; 20: 902–918. doi:10.1007/s11307-018-1265-0

[21] Haacke EM, Xu Y, Cheng YCN et al. Susceptibility weighted imaging (SWI). Magn Reson Med 2004; 52: 612–618. doi:10.1002/mrm.20198

[22] Hargreaves BA, Worters PW, Pauly KB et al. Metal-Induced Artifacts in MRI. American Journal of Roentgenology 2011; 197: 547–555. doi:10.2214/AJR.11.7364

[23] Ariyanayagam T, Malcolm PN, Toms AP. Advances in Metal Artifact Reduction Techniques for Periprosthetic Soft Tissue Imaging. Semin Musculoskelet Radiol 2015; 19: 328–334. doi:10.1055/s-0035-1563734

[24] Jungmann PM, Agten CA, Pfirrmann CW et al. Advances in MRI around metal. J Magn Reson Imaging 2017; 46: 972–991. doi:10.1002/jmri.25708

[25] Khodarahmi I, Isaac A, Fishman EK et al. Metal About the Hip and Artifact Reduction Techniques: From Basic Concepts to Advanced Imaging. Semin Musculoskelet Radiol 2019; 23: e68–e81. doi:10.1055/s-0039-1687898

[26] Harris CA, White LM. Metal Artifact Reduction in Musculoskeletal Magnetic Resonance Imaging. Orthopedic Clinics of North America 2006; 37: 349–359. doi:10.1016/j.ocl.2006.04.001

[27] Choi SJ, Koch KM, Hargreaves BA et al. Metal Artifact Reduction With MAVRIC SL at 3-T MRI in Patients With Hip Arthroplasty. American Journal of Roentgenology 2014; 204: 140–147. doi:10.2214/AJR.13.11785

[28] Guermazi A, Miaux Y, Zaim S et al. Metallic Artefacts in MR Imaging: Effects of Main Field Orientation and Strength. Clinical Radiology 2003; 58: 322–328. doi:10.1016/S0009-9260(02)00540-8

[29] Tartaglino LM, Flanders AE, Vinitski S et al. Metallic artifacts on MR images of the postoperative spine: reduction with fast spin-echo techniques. Radiology 1994; 190: 565–569. doi:10.1148/radiology.190.2.8284417

[30] Thompson RM, Fowler E, Culo B et al. MRI safety and imaging artifacts evaluated for a cannulated screw used for guided growth surgery. Magnetic Resonance Imaging 2020; 66: 219–225. doi:10.1016/j.mri.2019.11.005

[31] Ganapathi M, Joseph G, Savage R et al. MRI Susceptibility Artefacts Related to Scaphoid Screws: the Effect of Screw Type, Screw Orientation and Imaging Parameters. Journal of Hand Surgery 2002; 27: 165–170. doi:10.1054/JHSB.2001.0717

[32] Lee MJ, Kim S, Lee SA et al. Overcoming Artifacts from Metallic Orthopedic Implants at High-Field-Strength MR Imaging and Multi-detector CT. RadioGraphics 2007; 27: 791–803. doi:10.1148/rg.273065087

[33] Chiba Y, Murakami H, Sasaki M et al. Quantification of metal-induced susceptibility artifacts associated with ultrahigh-field magnetic resonance imaging of spinal implants. JOR Spine 2019; 2: doi:10.1002/jsp2.1064

[34] Sutter R, Dietrich T. Reduktion von Metallartefakten in der muskuloskelettalen Bildgebung. Radiologie up2date 2016; 16: 127–144. doi:10.1055/s-0042-105421

[35] Ladd ME, Erhart P, Debatin JF et al. Biopsy needle susceptibility artifacts. Magnetic Resonance in Medicine 1996; 36: 646–651. doi:10.1002/mrm.1910360423

[36] Faulkner W. Managing Metallic Artifacts in MRI. Im Internet: http://www.medtronic.me/content/dam/medtronic-com/ca-en/hcp/documents/MRI/Managing%20Metallic%20Artifact%20White%20Paper%20201604693EC.pdf

[37] Talbot BS, Weinberg EP. MR Imaging with Metal-suppression Sequences for Evaluation of Total Joint Arthroplasty. RadioGraphics 2016; 36: 209–225. doi:10.1148/rg.2016150075

[38] Stumpf K, van Gorp S, Strom A et al. Multi-sequence comparison of metal artifact reduction capabilities for dental materials. In: Proceedings of the Joint Annual Meeting of ISMRM and ESMRMB. Paris 2018

[39] Hövener JB, Zwick S, Leupold J et al. Dental MRI: imaging of soft and solid components without ionizing radiation. J Magn Reson Imaging 2012; 36: 841–846. doi:10.1002/jmri.23712

[40] Koch KM, Hargreaves BA, Pauly KB et al. Magnetic resonance imaging near metal implants. J Magn Reson Imaging 2010; 32: 773–787. doi:10.1002/jmri.22313

[41] Jiang M, He C, Feng J et al. Magnetic resonance imaging parameter optimizations for diagnosis of periprosthetic infection and tumor recurrence in artificial joint replacement patients. Sci Rep 2016; 6: 36995 doi:10.1038/srep36995

[42] Viano AM, Gronemeyer SA, Haliloglu M et al. Improved MR imaging for patients with metallic implants. Magnetic Resonance Imaging 2000; 18: 287–295. doi:10.1016/S0730-725X(99)00135-6

[43] Kumar NM, de Cesar Netto C, Schon LC et al. Metal Artifact Reduction Magnetic Resonance Imaging Around Arthroplasty Implants: The Negative Effect of Long Echo Trains on the Implant-Related Artifact. Investigative Radiology 2017; 52: 310–316. doi:10.1097/RLI.0000000000000350

[44] de Cesar Netto C, Fonseca LF, Fritz B et al. Metal artifact reduction MRI of total ankle arthroplasty implants. Eur Radiol 2018; 28: 2216–2227. doi:10.1007/s00330-017-5153-9

[45] Ramos-Cabrer P, van Duynhoven JPM, Van der Toorn A et al. MRI of hip prostheses using single-point methods: In vitro studies towards the artifact-free imaging of individuals with metal implants. Magnetic Resonance Imaging 2004; 22: 1097–1103. doi:10.1016/j.mri.2004.01.061

[46] Cho ZH, Kim DJ, Kim YK. Total inhomogeneity correction including chemical shifts and susceptibility by view angle tilting: Total inhomogeneity correction including chemical shift. Med Phys 1988; 15: 7–11. doi:10.1118/1.596162

[47] Reichert M, Ai T, Morelli JN et al. Metal artefact reduction in MRI at both 1.5 and 3.0 T using slice encoding for metal artefact correction and view angle tilting. BJR 2015; 88: 20140601 doi:10.1259/bjr.20140601

[48] Olsen RV, Munk PL, Lee MJ et al. Metal Artifact Reduction Sequence: Early Clinical Applications. RadioGraphics 2000; 20: 699–712. doi:10.1148/radiographics.20.3.g00ma10699

[49] Toms AP, Smith-Bateman C, Malcolm PN et al. Optimization of metal artefact reduction (MAR) sequences for MRI of total hip prostheses. Clinical Radiology 2010; 65: 447–452. doi:10.1016/j.crad.2009.12.014

[50] Lu W, Pauly KB, Gold GE et al. SEMAC: Slice encoding for metal artifact correction in MRI. Magn Reson Med 2009; 62: 66–76. doi:10.1002/mrm.21967

[51] Deligianni X, Bieri O, Elke R et al. Optimization of Scan Time in MRI for Total Hip Prostheses: SEMAC Tailoring for Prosthetic Implants Containing Different Types of Metals. Rofo 2015; 187: 1116–1122. doi:10.1055/s-0041-104893

[52] Koch KM, Lorbiecki JE, Hinks RS et al. A multispectral three-dimensional acquisition technique for imaging near metal implants. Magn Reson Med 2009; 61: 381–390. doi:10.1002/mrm.21856

[53] Koch KM, Brau AC, Chen W et al. Imaging near metal with a MAVRIC-SEMAC hybrid. Magnetic Resonance in Medicine 2011; 65: 71–82. doi:10.1002/mrm.22523

[54] O-MAR | Klinische MR-Anwendung | Philips Healthcare. Philips. Im Internet (Stand: 22.07.2020): https://www.philips.de/healthcare/product/HCNMRB815/O-MAR-MR-Software

[55] WARP. Im Internet (Stand: 22.07.2020): https://www.siemens-healthineers.com/de/medical-imaging/magnetic-resonance-imaging/options-and-upgrades/clinical-applications/syngo-warp/features

[56] O-MAR XD | Klinische MR-Anwendung | Philips Healthcare. Philips. Im Internet (Stand: 22.07.2020): https://www.philips.de/healthcare/product/HCNMRB816A/O-MAR-XD-MR-Software

[57] Advanced WARP. Im Internet (Stand: 22.07.2020): https://www.siemens-healthineers.com/de/medical-imaging/magnetic-resonance-imaging/options-and-upgrades/clinical-applications/advanced-warp/features

[58] Duong STM, Phung SL, Bouzerdoum A et al. An unsupervised deep learning technique for susceptibility artifact correction in reversed phase-encoding EPI images. Magnetic Resonance Imaging 2020; 71: 1–10. doi:10.1016/j.mri.2020.04.004

[59] Kwon K, Kim D, Kim B et al. Unsupervised learning of a deep neural network for metal artifact correction using dual-polarity readout gradients. Magnetic Resonance in Medicine 2020; 83: 124–138. doi:10.1002/mrm.27917